Phase behavior in thin films of cylinder-forming *ABA* block copolymers: Experiments

Armin Knoll[a] and Robert Magerle[b]
Lehrstuhl für Physikalische Chemie, II, Universität Bayreuth, 95440 Bayreuth, Germany

Georg Krausch
Lehrstuhl für Physikalische Chemie II and Bayreuther Zentrum für Kolloide und Grenzflächen (BZKG), Universität Bayreuth, 95440 Bayreuth, Germany

(Received 24 June 2003; accepted 25 September 2003)

We experimentally establish a phase diagram of thin films of concentrated solutions of a cylinder forming polystyrene-*block*-polybutadiene-*block*-polystyrene triblock copolymer in chloroform. During annealing the film forms islands and holes with energetically favored values of film thickness. The thin film structure depends on the local thickness of the film and the polymer concentration. Typically, at a thickness close to a favored film thickness parallel orientation of cylinders is observed, while perpendicular orientation is formed at an intermediate film thickness. At high polymer concentration the cylindrical microdomains reconstruct to a perforated lamella structure. Deviations from the bulk structure, such as the perforated lamella and a wetting layer are stabilized in films thinner than ≈1.5 domain spacings. © *2004 American Institute of Physics.*
[DOI: 10.1063/1.1627324]

I. INTRODUCTION

Supramolecular self-assembly is widely used in nature to build highly regular and complex structures with dimensions much larger than the dimensions of the molecules. Block copolymers are an interesting model system to study this phenomenon because one is able to precisely control the architecture of the molecules. Furthermore these systems self-assemble into patterns with length scales of 5–100 nm, which might be interesting for a variety of applications, for instance, lithographic masks[1–6] and templates for nanostructured inorganic materials.[7–9] For a popular review on these topics, see Ref. 10.

A block copolymer is built from two or more polymeric chains (blocks), which are chemically different and covalently attached to each other. Their phase behavior is controlled by the interaction between the blocks and the relative lengths of the blocks. If the incompatibility is large enough the polymer microphase separates and forms ordered structures depending on the relative volume fraction of the blocks, e.g., lamellae, gyroid, cylinders, or spheres. The size of the nanostructures can be adjusted within a certain range by the overall molecular weight of the block copolymer (for recent reviews, see Refs. 10–12) and by addition of homopolymer.[13,14] An interesting application of these features is the use of block copolymer films for lithographic purposes[2–6] and/or templating of inorganic structures.[7–9] The patterns may be aligned by the use of external electric fields,[15] topographic templating,[16] and surface patterning.[17] All these processes rely on the control of pattern formation of the block copolymer in thin films and therefore on a good understanding of the underlying physics.

The presence of a surface or interface is known to influence the microdomain structure in the vicinity of the surface, even if the bulk is not ordered.[18] Generally, the block with the lower surface energy tends to accumulate at the surface. This preferential attraction to the surface (the surface field) typically leads to an alignment of the structure (lamellae, layers of cylinders, layers of spheres) parallel to the interface. In some cases this alignment extends over a large distance into the bulk of the material.[19] In addition to alignment, the presence of a surface can also modify the microdomain structure close to the surface, similar to surface reconstructions known from classical solid state physics. This has first been observed for cylinder forming systems. If the minority component has a sufficiently lower surface energy than the majority component, a wetting layer is formed at the surface allowing the low surface energy phase to completely cover the surface.[20] In the opposite case, when the majority component is favored at the surface, it was predicted that the cylinders next to the surface may transform to one layer of a perforated lamella[21,22] or a lamella.[23] In lamella forming *ABC* triblock copolymers a complex surface reconstruction was observed for the case that the middle block has the lowest surface energy.[24,25]

In a thin film the copolymer material is confined to a certain film thickness, which gives rise to additional effects: If the film thickness deviates from an integer multiple of the characteristic spacing, the microdomains need to thicken or compress, which leads to an increase of the free energy by entropic contributions. Therefore supported as well as free standing films form regions of different film thickness (terraces), which correspond to an integer multiple of the natural microdomain layer spacing. This has been observed for lamella,[26] cylinder,[27] and sphere[19] forming systems.

If the film is not free to adjust its local film thickness,

[a]Electronic mail: armin.knoll@uni-bayreuth.de
[b]Electronic mail: robert.magerle@uni-bayreuth.de

i.e., in the case of two solid interfaces, the difference in the interfacial tension of the blocks controls the thin film behavior. For lamella forming systems a large surface field forces the lamellae to stretch and adapt a new, commensurable layer spacing.[28] In the case of a weak surface field, lamellae oriented perpendicular to the substrate.[29,30] In cases where the two interfaces favor different orientations, both can coexist and a mixed (hybrid) microdomain structure is stabilized.[31,32]

Cylinder forming block copolymers show a more complex phase behavior in thin films. In the case of a weak surface field, the bulk microdomain structure is not significantly altered and the orientation behavior of cylinders is analogous to lamella forming systems. When the surfaces preferentially attract the majority block, the cylinders align parallel to the substrate.[27,33–35] Otherwise, half cylinders may form.[36] A perpendicular orientation of cylinders, however, has been stabilized only with the help of an electric field[8] or by fast drying in solvent cast films.[34,35,37]

In the case of strong surface fields, a variety of deviations from the bulk structures has been observed. If the minority block has the lower surface energy a transformation to a wetting layer (a half lamella)[20] and a lamella[38] have been observed in very thin films. If the majority block is accumulated at the surface, a perforated lamellar phase has been reported in free standing films.[38] Also mixed (or hybrid) structures, such as cylinders with necks[39] and spheres on top of a perforated lamella layer[40] as well as an ''inverted phase''[41] have been observed. Furthermore, in films thinner than a natural microdomain spacing, a disordered phase was observed.[42] Various models have been developed[21–23,43–48] to describe different aspects of this complex phase behavior. However, it remained unclear which of the reported phenomena are specific to the particular system and/or route of film preparation and which are general behavior.

In a previous letter we presented a unifying description of the phase behavior in thin films of cylinder forming block copolymers.[49] With experiments and computer simulations based on dynamic density functional theory we showed that the phase behavior in thin films of cylinder forming block copolymers can be understood by the interplay between surface reconstructions and confinement effects. In this paper we give a full account on the experimental part of our work. A full account on the corresponding simulation results is given in a separate article.[50]

The outline of the paper is as follows: We first show that chloroform is a nonselective solvent for our system, which does not alter the bulk microdomain structure of our polymer in the considered range of dilution. Therefore it merely introduces mobility to our system. We show how the thin film forms regions of preferred thickness to minimize its free energy. *In situ* measurements prove the existence of microphase separation inside the thin films during annealing, i.e., in the swollen state. They also show that the microdomain structure is preserved during the drying process of the swollen films. We then systematically analyze and identify the microdomain structure as a function of film thickness and polymer concentration and establish a phase diagram for our system.

II. EXPERIMENT

A. Materials

We have studied thin films of a polystyrene-*block*-polybutadiene-*block*-polystyrene (SBS) triblock copolymer swollen in chloroform vapor. SBS was obtained from Polymer Source Inc. with molecular weights $M_{w,\mathrm{PS}}=14\,\mathrm{kg/mol}$, $M_{w,\mathrm{PB}}=73\,\mathrm{kg/mol}$, and $M_{w,\mathrm{PS}}=15\,\mathrm{kg/mol}$ (PS is polystyrene, PB is polybutadiene). Taking into account the densities of the homopolymers (1.05 g/cm^3 for PS and 0.93 g/cm^3 for PB)[51] the volume fraction of PS is $\Phi_{\mathrm{PS}}=0.26$. PS and PB homo-polymers used for ellipsometry were obtained from Polymer Standard Service (Mainz, Germany) with molecular weights of $M_{w,\mathrm{PS}}=520\,\mathrm{kg/mol}$ and $M_{w,\mathrm{PB}}=47\,\mathrm{kg/mol}$.

For scanning force microscopy (SFM) and ellipsometry experiments, polished silicon substrates were cut from wafers, cleaned in fresh 1:1 H_2SO_4(conc.)/H_2O_2 (30%) solution, thoroughly rinsed in boiling and cold Millipore water, and finally cleaned with a Snowjet®.

B. Small angle x-ray scattering

The bulk microdomain structure of concentrated SBS solutions in chloroform was investigated using small angle x-ray scattering (SAXS). All measurements were performed at the ID2A beamline at the European Synchrotron Radiation Facility (ESRF, Grenoble, France). The energy of the beam was set at 12.5 keV. SAXS spectra were measured of SBS solutions in chloroform at different polymer weight fractions. Solutions of 30, 40, and 50 wt % SBS and a bulk sample were prepared. Dilute solutions were either injected into a chamber with microscope slides as windows (30 wt %) or directly prepared in capillaries with 2 mm diameter (30 and 40 wt %). At high concentrations (40 and 50 wt %) injection was not possible due to the high viscosity of the solution. For these concentrations a droplet of the solution was put directly into the beam and immediately measured. The bulk sample was prepared by slowly drying a SBS solution inside a capillary. Due to the high scattering cross section of the chlorine atoms and the long pathway for the beam through the chamber of 5 mm, imaging times of 3–5 s had to be chosen for the samples not prepared in capillaries.

C. Thin film preparation

For ellipsometry measurements, polymer films of PS, PB, and SBS were spin-cast from toluene solutions (2 wt %) yielding an initial film thickness of about 125 nm.

To study the thin film phase behavior of SBS, films were spun cast from toluene solution onto polished silicon substrates. Solutions with 0.25, 0.5, 0.75, 1, 1.5, and 2 wt % SBS and a spinning speed of 2000 rpm were used. This procedure resulted in films with a thickness of about 12, 25, 35, 50, 80, and 125 nm, respectively, and with a surface roughness of less than 1 nm as measured by SFM. In order to equilibrate (anneal) the microdomain structure, the films were exposed for several hours to a controlled partial pressure p of chloroform vapor. The experimental setup is shown in Fig. 1. Two flows of nitrogen gas, one saturated with chloroform vapor in a washing bottle, are mixed just before entering the sample

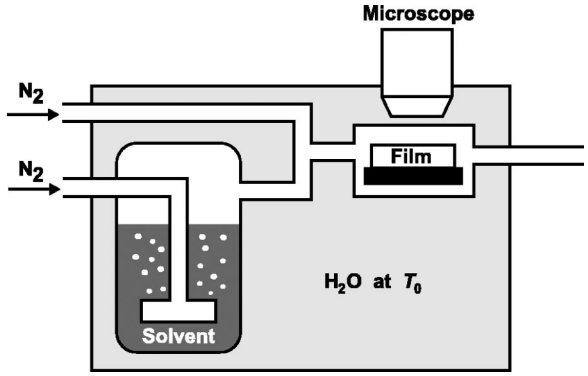

FIG. 1. Sketch of the experimental setup for swelling in chloroform vapor. Two flows of air or N_2 are mixed, one of them is saturated by $CHCl_3$ vapor by passing it through a washing-bottle. The flow ratio of the two gas streams determines the vapor pressure in the sample chamber. The sample can be viewed with an optical microscope to follow terrace formation. After annealing, the sample is quickly removed from the vapor in order to quench the microdomain structure.

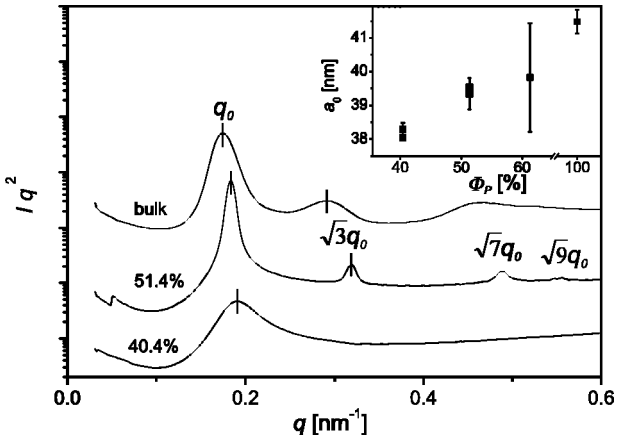

FIG. 2. SAXS spectra from bulk SBS and SBS/$CHCl_3$ solutions with polymer volume fractions $\Phi_p = 40.4\%$ and 51.4%. The scattering peaks typical for a microdomain structure of hexagonally ordered cylinders are marked. The inset shows the spacing a_0 between next-nearest cylinders as a function of Φ_p.

chamber. The volume flow for each line was regulated via flow-meters and ranged from 20 to 50 cm^3/min. The whole setup was made from glass using Teflon™ connectors. It was inserted into a water bath kept at $T_0 = 25.0 \pm 0.1\,^\circ$C. An overpressure of 0.3 ± 0.1 bar was applied to the system to detect possible leakage. The samples were placed onto a glass slide welded to a flange, which could be quickly removed from the chamber after equilibration to extract the solvent and quench the microdomain structure.

D. Spectroscopic ellipsometry

We used ellipsometry to determine the amount of chloroform within the polymer films at a given chloroform vapor pressure. All measurements were done on a SENTECH SE 850 spectroscopic ellipsometer. A homemade setup[52] was used to establish an atmosphere with a controlled solvent vapor pressure. The temperature of the sample and the temperature of a solvent reservoir were controlled to within 0.1 K. All measurements were performed at 65° incidence angle within a spectral range from 400 to 800 nm. The thickness d at a certain vapor pressure p was obtained from least-squares fits to the spectral data of the ellipsometer. Hereby the block copolymer film is modeled as a homogeneous material with an effective refractive index $n(\lambda) = n_0 + n_1\,100/(\lambda/\mathrm{nm}) + n_2\,10^7/(\lambda/\mathrm{nm})^2$ where λ is the wavelength and n_0, n_1, and n_2 are fitting parameters (Cauchy model); the absorption in the film was assumed to be negligible. The thickness of all films was measured upon swelling and deswelling of the sample to rule out possible hysteresis effects. Before and after measuring in solvent vapor, the thickness d_0 of the dry samples was measured. The polymer concentration Φ_p in the film is given by

$$\Phi_p = \frac{d_0}{d},$$

assuming that the partial volumes of polymer and solvent in the film are additive.

To measure the polymer volume fraction Φ_p as a function of vapor pressure p under the conditions used for thin film preparation, the above-described flow setup was connected to the ellipsometer cell and the same overpressure and temperature were applied (not shown here). Φ_p was measured for all combinations of gas flows applied during sample preparation.[53]

E. Scanning force microscopy

The microdomain structures at the surface of the dry films were imaged with a Dimension 3100 Metrology SFM from Digital Instruments, Veeco Metrology Group and a Nanoscope IIIm controller. Some data were taken using a Dimension 3100. The metrology system uses a hardware linearized piezo scanner, which allows very accurate measurements of distances and heights from the images. Both instruments were operated in tapping mode. Olympus and Nanosensors tapping mode cantilevers were used (spring constant ≈40 N/m, resonance frequency ranging from 200 to 300 kHz). All measurements were performed at free amplitudes of about 30–50 nm and a relative setpoint of about 0.95. Some experiments were performed in the presence of chloroform vapor (see Sec. III D for details).

III. RESULTS

A. Domain spacing in bulk SBS solutions

To measure the microdomain spacing of the copolymer solutions in bulk samples, we have performed synchrotron SAXS measurements at copolymer concentrations of 30, 40, and 50 wt % and for a bulk sample. The corresponding polymer volume fractions of the solutions amount to $\Phi_p = 0.40$, 0.51, and 0.61, respectively. The two-dimensional-SAXS images were averaged azimuthally. The results obtained for the solutions prepared in the capillaries are shown in Fig. 2. From the first-order scattering peak at q_0, the spacing between layers of cylinders can be extracted as $c_0 = 2\pi/q_0$. While the curve measured for $\Phi_p = 0.40$ shows a rather broad first order peak and no higher order peaks, the spectrum measured at $\Phi_p = 0.51$ shows a narrow first-order peak and three higher order peaks at $\sqrt{3}\,q_0$, $\sqrt{7}\,q_0$, and $\sqrt{9}\,q_0$

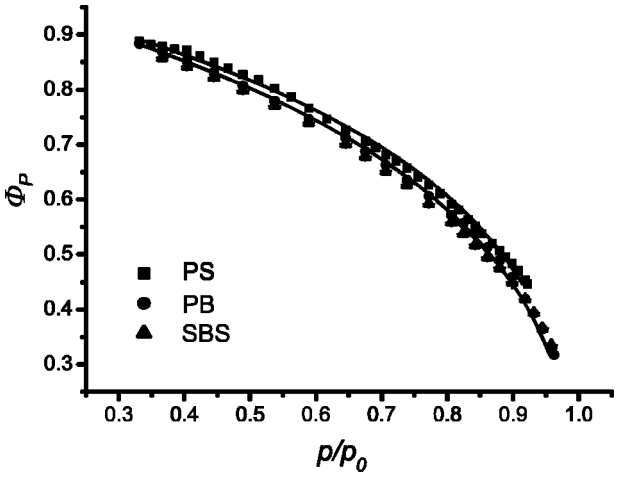

FIG. 3. Polymer volume fraction Φ_p as a function of the relative $CHCl_3$ vapor pressure of swollen films of polystyrene, polybutadiene, and the triblock copolymer SBS. The lines show fits of the measured data with a simple model (see Sec. III B).

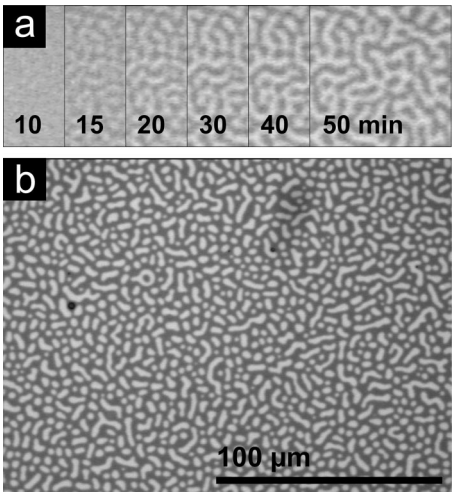

FIG. 4. (a) Optical micrographs of swollen films as a function of annealing time, visualizing the terrace formation. Terraces with different film thickness are visible because of interference of light scattered by the surface of the film and the substrate. The time scale of terrace formation depends on the vapor pressure and on the initial thickness of the film. (b) Image of the quenched film after 7 h of annealing. It shows that terraces extend over large areas of the sample.

characteristic for hexagonally packed cylinders. Since the bulk sample still shows one higher order peak at $\sqrt{3}\,q_0$, we consider a bulk microdomain structure of hexagonally ordered cylinders throughout the concentration regime used in this study for the thin film.

The inset to Fig. 2 shows the next nearest neighbor spacing between cylinders $a_0 = 2/\sqrt{3}\,c_0$ as a function of Φ_p for all samples prepared. The spacing increases with increasing polymer concentration. Within the concentration regime studied here, a_0 increases from 38.0 ± 0.3 to 41.5 ± 0.4 nm. The large error bar at $\Phi_p = 0.51$ results from a highly distorted, elliptic scattering image due to difficult sample preparation at high Φ_p.

B. Swelling behavior and molecular interactions in thin SBS films

In order to quantify the polymer volume fraction within the thin films at a given solvent vapor pressure, we have measured the film thickness in the swollen state for films of PS and PB homopolymers, and SBS block copolymer. The solvent pressure was controlled by keeping the sample at 25 °C and adjusting the temperature of a solvent reservoir inside the chamber to a lower temperature. With increasing solvent vapor pressure p the film takes up more solvent, i.e., Φ_p decreases (Fig. 3). PB films swell by only about 3% more than PS films at a given chloroform vapor pressure. This shows that chloroform is a good solvent for both polymers, exhibiting only a small selectivity to PB. SBS takes up slightly more solvent than the respective homopolymers possibly due to an enrichment of solvent at the polymer–polymer interfaces, which thereby screens repulsive interactions between the S and B monomers.[54]

The swelling behavior of PS and PB homopolymers can be modeled with Flory–Huggins theory.[55] If we denote the vapor pressure at saturation as p_0, the chemical potential in the vapor phase is given by $\mu_v = \ln(p/p_0)$. A comparison to the chemical potential in the thin film μ_s, given by Flory–Huggins theory,[55] yields the following relation between the normalized vapor pressure p/p_0 and the polymer volume fraction Φ_p:

$$\ln(p/p_0) = \frac{\mu_v}{RT} = \frac{\mu_s}{RT} = \chi_{P,S}\Phi_p^2 + \ln(1-\Phi_p) + (1-1/N)\Phi_p .$$

N is the total degree of polymerization and $\chi_{P,S}$ is the Flory–Huggins interaction parameter between polymer and solvent. Assuming that $\chi_{P,S}$ does not depend on Φ_p, the ellipsometric data can be fitted with a single parameter $\chi_{P,S}$. The results of least-squares fits are shown in Fig. 3 (solid lines) together with the data. The agreement between the fit and the data is very good. The resulting interaction parameters $\chi_{P,S}$ of 0.29 ± 0.01 for PS/$CHCl_3$ and 0.21 ± 0.1 for PB/$CHCl_3$ agree with the published values[51] in the respective concentration regime.

C. [5453]Coarse grain structure of the SBS films: Terrace formation

During annealing the swollen SBS films form islands and holes. Figure 4(a) shows a series of optical micrographs taken at different times of annealing. Within a time scale of about 1 h the initially flat film develops areas of uniform thickness characterized by uniform interference colors in the optical image [Fig. 4(b)]. This behavior is known from experiments of thin films of block copolymer melts.[26] It suggests that the local thickness adjusts to local minima of the free energy of the system, which are related to energetically preferred microdomain structures of the films. The initial film thickness was chosen such that islands and holes had similar area fractions at the applied solvent vapor pressure. Note that microphase separation inside the thin film is necessary to provide a driving force for terrace formation. Ter-

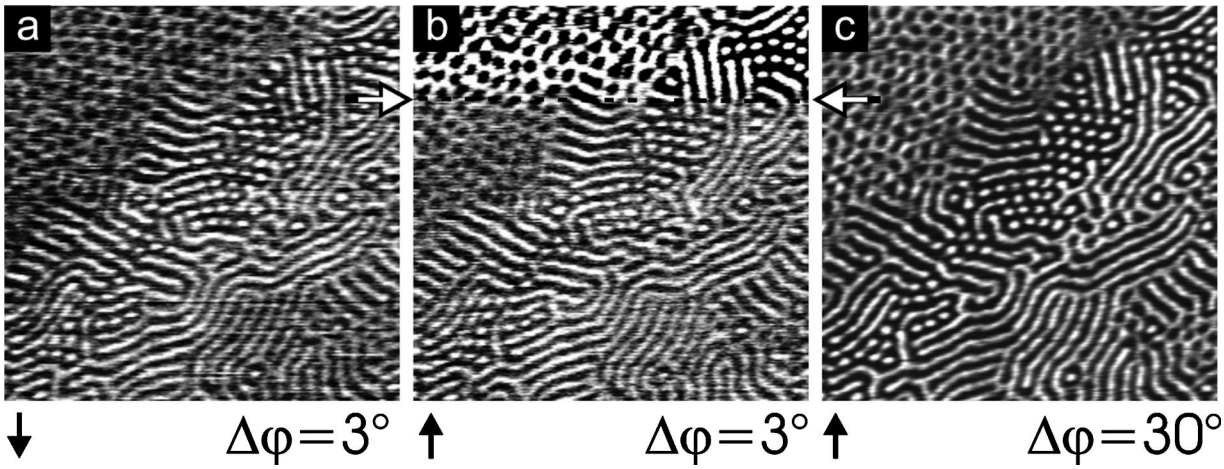

FIG. 5. *In situ* tapping mode SFM phase images (2×2 μm^2). The capture direction, the time relative to the start of the *in situ* experiment, and the range of the phase scale are denoted below the images. (a) Image taken during swelling at $p/p_0=0.65$ ($\Phi_p=0.7$). In the upper part of (b) (dark arrow) the drying process was started by switching to pure N_2 gas flow. (c) Image of the dry film. Note the change in the phase scale from 3° in the wet state to 30° in the dry state.

race formation has been observed for all samples with $\Phi_p<0.7$ during solvent annealing, indicating that the material inside the film is always well phase separated. Islands and holes formed in a very similar way in all samples irrespective of the film thickness except for the thickest films and the highest polymer volume fractions. In particular, at a film thickness of more than three layers of cylinders and at polymer volume fractions $\Phi_p>0.65$ no well defined terraces were formed within the time scale of the experiment.

Typically the terrace formation was faster at higher vapor pressures and for thinner films, but no systematic study on the kinetics of terrace formation has been performed. The films prepared by spin casting are somewhat thicker near the edges of the samples. In these regions a stepped surface structure with a larger number of different film thicknesses could be observed. During vapor treatment the films started to dewet. The annealing procedure was stopped either after roughly half of the film surface was dewetted or after 7 h of annealing.

D. Thin film microdomain structure

We performed *in situ* SFM measurements during sample preparation. Details of this experiment will be published elsewhere.[56] Figure 5 shows three consecutive SFM phase images taken at approximately $\Phi_P\approx0.7$ and during the drying process of the thin film. Although the phase contrast is rather small in the presence of chloroform, it clearly reveals the microdomain structure of the thin film. In this case the quench of the microdomain structure is done by switching to a pure N_2 gas flow. White arrows in Fig. 5(b) mark the position of the tip, when the gas flow has been switched. The strong increase in phase contrast renders the quick drying of the polymer film visible. Figure 5(c) was captured after drying of the film and readjustment of the tapping parameters. Comparison of the phase images demonstrates that the drying process does not alter the intrinsic structure of the microdomain pattern.

Figure 6 shows two SFM measurements of two samples

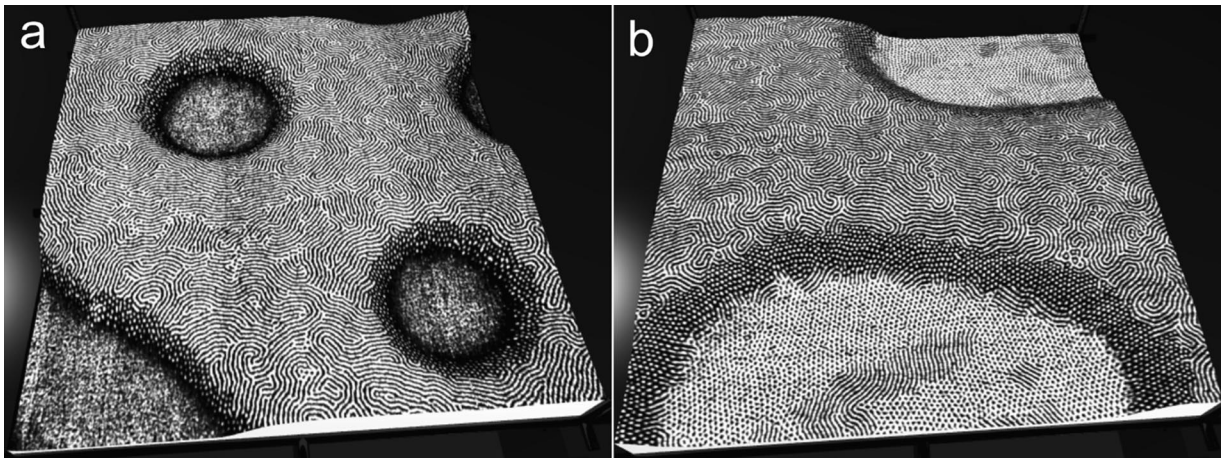

FIG. 6. Three-dimensional rendered SFM images (5×5 μm^2) using the height image as heightfield and the phase image as texture. The images show the formation of terraces in the film and the systematic change of microdomain structures along the changes in film thickness. (a) A film with 11- and 40-nm-thick terraces; (b) A film with 32 and 57-nm-thick terraces.

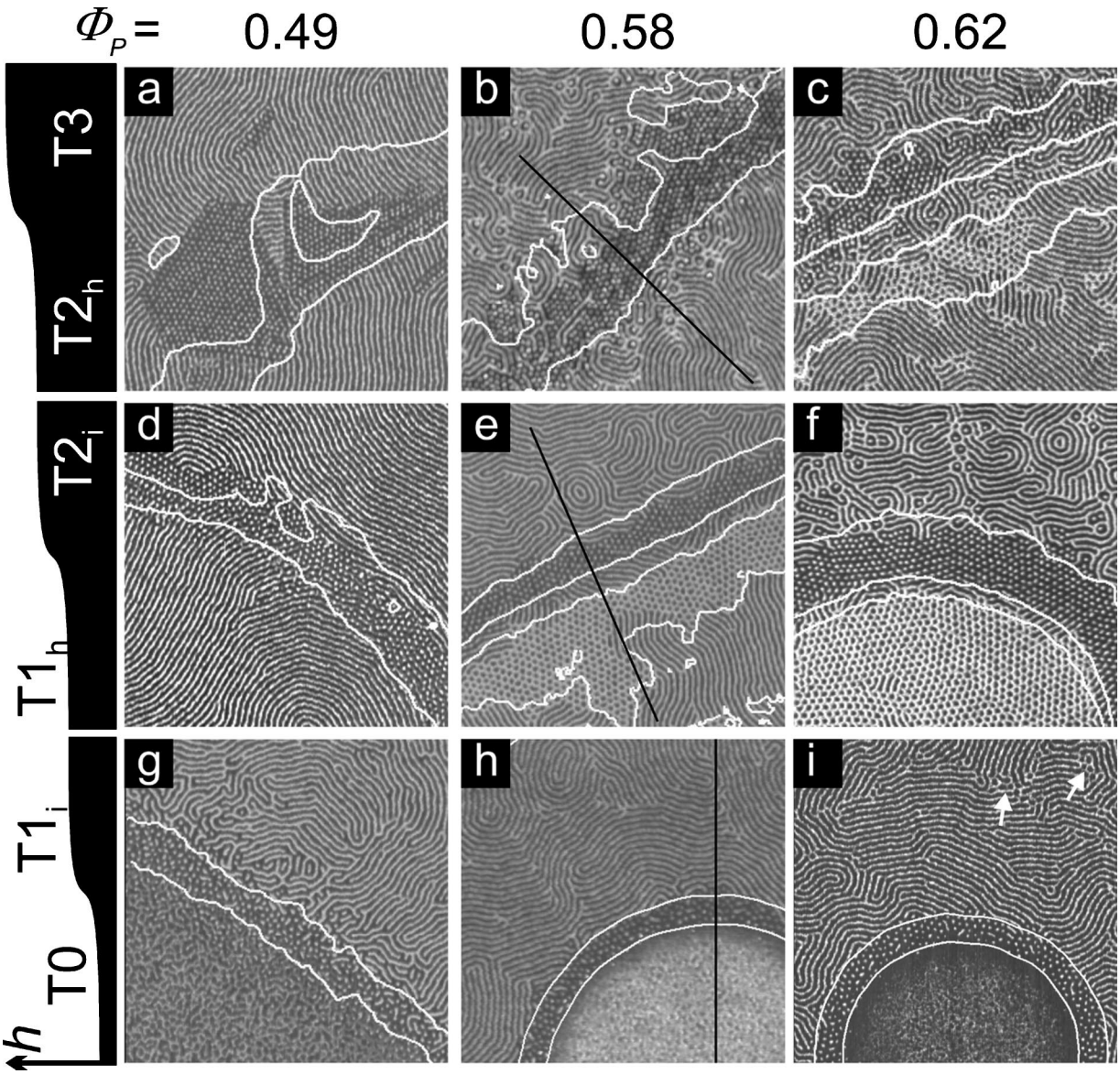

FIG. 7. SFM phase images at the edges of terraces as a function of film thickness h and polymer concentration Φ_p. Images are oriented such that the lower terrace is at the bottom in each image. Φ_p increases from left to right from 0.49, 0.58 to 0.62. From bottom to top the absolute height of the film increases. White lines correspond to contour lines, calculated from the corresponding height images, at which the microdomain structures change. Black lines indicate where the cross sections shown in Fig. 8 originate.

with different film thickness. The three-dimensional images were rendered with Pov-Ray™.[57] From the SFM height image the shape of the surface is calculated (''heightfield''), while the color information corresponds to the tapping mode phase image (''texture''). The images visualize simultaneously the existence of the terraces and the local microdomain structure in the film. The microdomain structure changes at distinct values of film thickness. In particular, different microdomain structures are found within the holes, at the steps, and on top of the islands.

Figure 7 shows nine SFM tapping mode phase images of annealed films with different polymer concentration and different film thickness: The film thickness increases from bottom to top and the polymer volume fraction Φ_p increases from left to right. Samples with different initial film thickness around $0.5\,c_0$ (bottom row), $1.5\,c_0$ (middle row), and $2.5\,c_0$ (top tow) are shown. On exposure to chloroform vapor, the films form terraces of well-defined thickness, which we will refer to as T0, T1, T2, and T3, respectively. See the sketch to the left of Fig. 7 for the variation of the film thickness and the numbering of the different terraces. The images in Fig. 7 are oriented such that the lower terrace always lies to the bottom of the image. Thereby, corresponding terraces Tn formed as holes from initially thicker films and as islands from initially thinner films are located next to each other in Fig. 7. Although their thickness is equal to within the experimental error, we observe different behavior depending on whether a given terrace was formed as a hole or as an island. Therefore we distinguish between Tn_h and Tn_i, respectively. The reason for the different behavior of the two terraces is most likely a tiny difference in film thickness and not the different route of formation. We will come back to this issue in more detail below. All images have a size of $2\times2\ \mu\text{m}^2$ and were recorded at an arbitrarily chosen edge of islands and

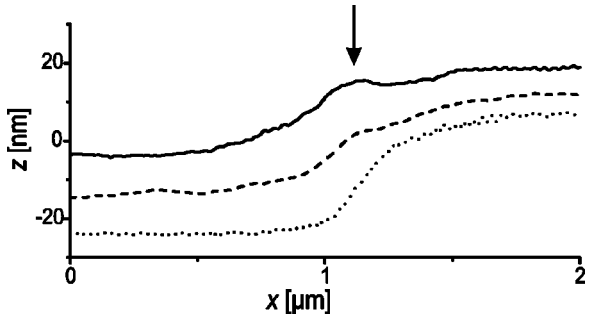

FIG. 8. Cross sections across terrace steps of the height images corresponding to the dark lines shown in Figs. 7(b), 7(e), and 7(h) (solid, dashed, and dotted curve, respectively). The thickest film shows a local maximum along the step profile. This is attributed to the fact that the $C_\perp$ phase shrinks less than the $C_\parallel$ phase during the drying process.

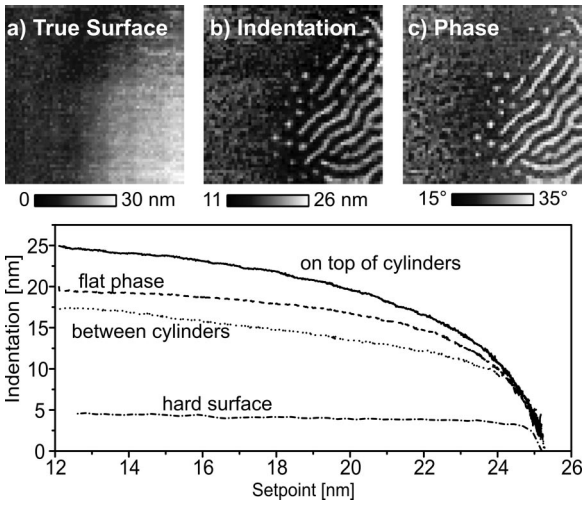

FIG. 9. True Surface SFM of a thin SBS film. (a) Reconstructed True Surface image of a terrace edge. The surface is locally flat with no sign of a lateral structure corresponding to the underlying microdomain structure. (b) Indentation image and (c) phase image at a relative set-point of 0.7. The comparison of both images shows that harder regions (less indentation) appear bright in the phase image. (d) Averaged amplitude-phase-distance (APD) curves of selected regions in the image. At least three curves were averaged. For comparison an APD curve for a hard polymeric surface is shown.

holes. Height images are not shown, for they are very similar to the ones used in Fig. 6. White contour lines calculated from the height images are superimposed onto the phase images. They clearly demonstrate that the boundaries between different structures always appear at a well-defined film thickness. Cross sections of the height image taken along the black lines shown in Figs. 7(b), 7(e), and 7(h) are shown in Fig. 8. The images show systematic changes in the microdomain patterns. Four characteristic patterns can be distinguished at the film surfaces: A stripe pattern, which we identify as PS cylinders aligned parallel to the plane of the film ($C_\parallel$), a pattern of hexagonally ordered bright dots originating from perpendicularly oriented PS cylinders ($C_\perp$), a pattern of hexagonally ordered dark dots corresponding to a perforated PS lamella (PL), and a rather featureless pattern, which we identify with a disordered phase (dis). The assignment of the surface patterns to three-dimensional microdomain structures is based on results of computer simulations,[49,50] on Nanotomography experiments,[39,58] and on True Surface measurements.[59] They will be discussed in more detail in the following. The terraces of larger thickness usually exhibit $C_\parallel$, which extends over larger areas and has a better long range order at a low polymer concentration. In all images $C_\perp$ appears in the regions between holes and islands. At high Φ_p, PL appears at the rim of the lower terrace $T1_h$, extending over the entire terrace at very high Φ_p. The lowest terrace shows a disordered pattern (dis). This pattern shows more pronounced lateral features at low Φ_p.

The contour lines mark the border between different patterns quite accurately. This is particularly the case at low thickness, at the border from $C_\parallel$ to $C_\perp$. Figure 8 shows three cross sections of the height image corresponding to the black lines displayed in Fig. 7. The local maximum in the step profile of the $C_\perp$ phase at high thickness is attributed to the fact that $C_\perp$ has an almost continuous phase of styrene throughout the entire thickness of the film. During drying of the film the PS-rich regions become glassy first, which causes this microdomain structure to shrink less than the other phases. Therefore, height lines do not fit to the border of the pattern in these cases [for example, in Figs. 7(a) and 7(b)].

With increasing polymer concentration Φ_p the perforated lamella morphology (PL) appears in thin films within the terraces formed as holes ($T1_h$,$T2_h$). Interestingly on islands, which exhibit the same thickness within experimental accuracy ($T1_i$,$T2_i$), this structure is only rarely observed and merely appears as a characteristic defect in the $C_\parallel$ phase [marked with white arrows in Fig. 7(i)]. At intermediate Φ_p, the perforated lamellar phase exists only near the edge of the hole. The thickness of these regions is a few nanometers larger than the thickness in the center of the respective terrace. The area fraction of the PL phase increases with Φ_p, until the entire terrace $T1_h$ is filled. The finding that PL appears predominantly in holes and at somewhat larger film thickness indicates that the favored thickness of the PL is a few nanometers larger than the one for $C_\parallel$. This is consistent with theoretical results, which predict a few percent increase of the characteristic domain spacing as one moves from cylindrical microdomains through the perforated lamella to the lamella at a given molecular weight.[60]

E. Identification of the microdomain structure

To unambiguously assign the observed patterns found on the film surfaces to distinct microdomain structures, we have identified the origin of the contrast observed in the SFM height and phase images and have measured the position of the true surface.[59] A laterally resolved array of 64×64 amplitude and phase versus distance (APD) curves was recorded. From each APD curve the z location of initial contact between tip and surface can be determined. This procedure allows one to determine the true shape of the surface irrespective of the tip indentation into the soft polymeric material. Moreover, indentation maps and phase images can be calculated from the APD data for any given setpoint A/A_0. Figure 9 shows a true surface image, an indentation image, and a phase image at a setpoint $A/A_0=0.7$. The indentation

curves in Fig. 9(d) show the indentation as a function of the amplitude setpoint. At the free amplitude of about 30 nm used in the experiments and at lower setpoints ($A/A_0 < 0.95$) repulsive interactions dominate over attractive forces and the indentation is higher on softer materials. Therefore, larger (smaller) indentations are related to soft, PB rich (glassy, PS rich) areas. When we compare the indentation and the phase images, we can clearly show that the brighter regions in the phase image correspond to the harder material, i.e., to PS-rich areas. The True Surface image is virtually flat on top of the terraces and does not reflect the microdomain structure. Together with the relatively large indentations at the given parameters this finding suggests that there is a PB-rich layer of about 10 nm thickness covering the entire sample surface (see Ref. 59 for details). This result is in agreement with the fact that PB has the lower surface energy of the two components ($\gamma_{PB}=30$ mN/m, Ref. 61; $\gamma_{PS}=41$ mN/m, Ref. 62) and a PB-rich surface layer is thermodynamically stable.

In summary, we can unambiguously identify the microdomain phases: From the SAXS and the Nanotomography experiments[58] we know that SBS forms hexagonally ordered cylinders in bulk and in thick films, respectively. The True Surface measurements allow us to identify the PS microdomains as bright structures in the phase images. They show further that the sample surface is covered by a PB layer of about 10 nm thickness. Additionally we can compare these results with recent calculations based on dynamic density functional theory (DDFT) using the MESODYN code, parts of which were published in Ref. 49 and which are discussed in more detail in Ref. 50. The excellent agreement between simulation and experimental results strongly corroborates the following identification of the microdomain structure: $C_{\parallel}$ corresponds to PS-rich cylinders (bright) in a PB-rich matrix oriented parallel to the surface, $C_{\perp}$ corresponds to cylinders oriented perpendicular to the surface (bright dots), and PL corresponds to a perforated PS lamella oriented parallel to the surface (bright continuous structure perforated by dark dots). The featureless pattern ''dis'' could either be attributed to a wetting layer (half lamella) or to a disordered phase, where microphase separation is suppressed by confinement of the material.[42]

An interesting detail of the microdomain structure is seen between the first layer of cylinders and the $C_{\perp}$ phase. Here the cylinders show undulations, which makes it difficult to define unambiguously the border between lines and dots in the phase images. We identify this structure as ''cylinders with necks,'' which have been found before in the same system[39] and can also be found in the DDFT simulations.[50]

F. Phase diagram

We construct a phase diagram by plotting the observed phases as a function of the film thickness and the polymer concentration in the films. To localize the boundaries between phases occurring at different film thickness, we determine the absolute values of the film thickness at the contour lines in the SFM images, where the lateral phase boundaries are located. To measure the absolute thickness of any given terrace a scratch was applied to the film with either a needle or a scalpel. Then a smooth edge of the scratch was chosen using an optical microscope and the step height was measured with SFM. Scan sizes between 5×5 and 20×20 μm^2 were chosen. Background subtraction was done by fitting a plane to the area in the image, where the bare silicon substrate is exposed. Close to the scratch, images with smaller scan sizes (between 3×3 and 5×5 μm^2) were taken at steps of the terraces to measure the existing microdomain phase patterns and their height relative to the terraces. Height histograms were calculated from the height images and background subtraction was optimized by maximizing the peaks in the height histogram. The lower peak was then taken as a reference and the relative heights were added to the absolute height of the corresponding lower terrace. By this procedure we determined the absolute heights h_{dry} of the different regions of the films after solvent extraction.

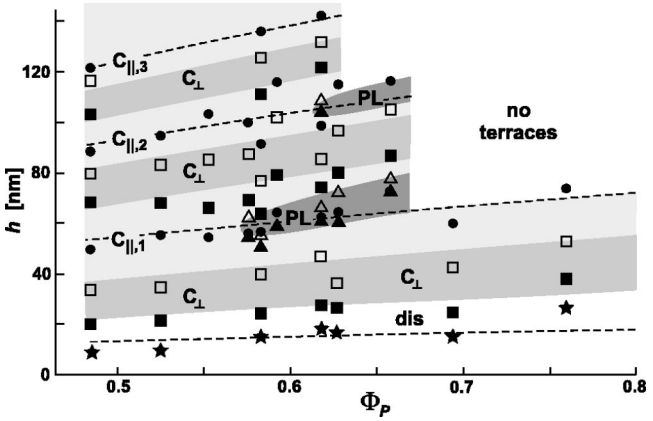

FIG. 10. Phase diagram of observed surface structures. Dashed lines correspond to functions $h=A\Phi_p^{0.6}$, with $A=20$, 82, 140 and 187 nm, representing the thickness of the terraces. Data are given for equilibrium film thicknesses of $C_{\parallel}$ (●) and ''dis'' (★) and for upper and lower bounds (open and closed symbols, respectively) of $C_{\perp}$ (□,■) and PL (△,▲) phases. The latter correspond to the height at contour lines such as those shown in Fig. 7. All lines and areas are drawn to guide the eye.

In order to account for the fact that the observed microdomain structures are formed in the swollen films, we calculate the thickness in the swollen state, $h_{wet}=h_{dry}/\Phi_p$, from h_{dry} as determined earlier and the polymer volume fraction Φ_p as determined with ellipsometry. The results are presented in Fig. 10 showing both the heights at which terraces form and the heights at which microdomain structures change. The heights of the terraces scale approximately with $\Phi_p^{0.6}$, which is indicated by the dashed lines in the diagram. This scaling is stronger in Φ_p than what is found for the scaling of lattice parameters of bulk solutions.[63–65] At very small film thicknesses we observe a disordered surface structure. We note that the height difference measured between the substrate and the first layer of cylinders (T1) amounts to about 60 nm, which appears very large for a single layer of cylinders with lateral spacing of about 40 nm. This finding indicates that the polymer layer found in the regions of smallest film thickness may extend over the entire substrate surface with the layers observed in thicker films being placed on top. Figure 11 shows the film thicknesses h_T of terraces formed on the rim of the sample for $\Phi_P=0.62$. h_T increases approximately linearly with the number of terraces as shown

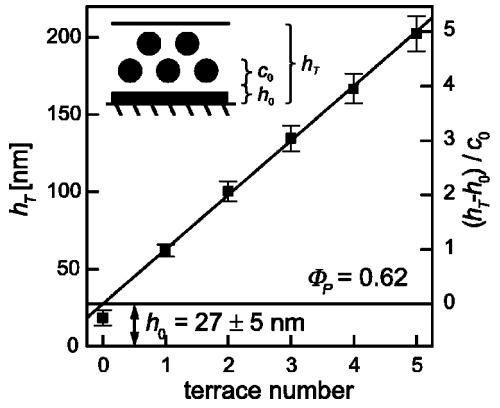

FIG. 11. Terrace height h_T and relative thickness of a cylinder layer $(h_T - h_0)/c_0$ as a function of terrace number, where c_0 denotes the natural layer thickness. The heights increase approximately linearly with the number of cylinder layers in the film. The offset h_0 of the plot at terrace number 0 corroborates the existence of a wetting layer with thickness h_0 underneath all films. The inset shows a sketch of this situation.

by the linear fit of the data with terrace number >0 (solid line). The data point given at terrace number 0 represents the thickness of the wetting layer. From the linear fit we determine a mean thickness of a cylinder layer c_0 to be 35 ± 2 nm, which fits well to the measured distance of in plane cylinders of about 39 nm. The linear fit suggests also an additional layer of material underneath the film of thickness $h_0=27 \pm 5$ nm, which corroborates the existence of a wetting layer everywhere at the film–substrate interface. This value is somewhat larger than the thickness of the ''dis'' phase of 18 ± 5 nm but also considerably smaller than c_0.

IV. DISCUSSION

Sample preparation in a controlled environment of solvent vapor gives additional insight into the phase behavior of thin block copolymer films. The volatile solvent chloroform is nonselective and merely enhances the mobility of polymer molecules in the system. Its high volatility enables us to quench the microdomain structure, which has developed during annealing. The control of the polymer concentration Φ_p allows us to vary the effective interactions between the two components and between the two components and the boundary surfaces. The polymer concentration Φ_p was chosen high enough that the block copolymer solutions were microphase separated in all experiments. The SAXS results, the formation of terraces even in the most diluted films, and the *in situ* observation of the microdomain structure corroborate this assumption. Note that this is very different from experiments done by Kim *et al.*,[34,35] who used the dynamics of solvent evaporation to control the resulting microdomain structure in their thin film. The key difference is that Kim *et al.* started solvent extraction from the one-phase region. Therefore structure formation took place during the drying process only and is largely influenced by the evaporation rate. Our system, in contrast, is well phase separated before drying and the dynamics of the polymers is too slow to follow the sudden quench of the system.

Furthermore, our system had sufficient time to equilibrate so that we can safely speak of equilibrium structures and call Fig. 10 a phase diagram. To clarify this, it is important to discriminate the different time and length scales. On long time scales (hours) and large length scales (several micrometers and more) the pattern of terraces (Fig. 4) is still coarsening and the film is not in equilibrium. This process is driven by the effective line tension between neighboring terraces of different film thickness. However, on much smaller length scales ($\sim$100 nm, corresponding to a few microdomains), the film thickness can be considered constant and several hours of annealing sufficient for such a small patch of the film to adopt the equilibrium structure corresponding to its local film thickness. This separation of time and length scales is very important and we used the observation of terrace formation on large length scales to conclude that the film had sufficient time to adopt locally its equilibrium structure. Since for high polymer concentrations $\Phi_p>0.75$ and thick films no terraces form, we have not plotted the surface structures of these specimens in Fig. 10.

On longer time scales, during the coarsening of the terrace pattern, the film thickness can change, however, with changing film thickness, the microdomain structure will adjust to the local film thickness at this particular spot of the specimen. This is confirmed by imaging with scanning force microscopy (similar as in Sec. III D) the microdomain dynamics during terrace formation. These experiments will be reported elsewhere.[56] To this end they confirm that in our experiments the film had sufficient time to adopt its equilibrium structure corresponding to its local film thickness. Therefore, the mapping of surface structure to the local film thickness, as shown in Fig. 10, represents the phase diagram of surface structures as function of film thickness and polymer concentration.

In all but the thinnest regions of the films, cylinders oriented parallel to the plane of the film ($C_{\parallel}$) dominate the SFM images. The parallel alignment of the cylinders is favored over the perpendicular orientation because of the preferential attraction of PB to the surface and a penalty for the additional unfavorable interfaces occurring at the ends of the upright cylinders. As a result, terraces with a thickness corresponding to an integer multiple of the cylinder layer spacing form spontaneously. This behavior is well known from lamella forming systems where the lamellae tend to orient parallel to the plane of the film and the local film thickness adjusts to a well-defined multiple of the lamellar spacing.[26]

In between neighboring terraces exhibiting parallel oriented cylinders we find regions where the cylinders are oriented perpendicular to the plane of the film. We anticipate that the formation of upright cylinders is energetically favorable over a compression or stretching of the parallel structures to a thickness significantly deviating from an integer multiple of the natural layer thickness. This notion is corroborated by the DDFT simulation results,[49,50] which also predict the formation of upright cylinders as a stable thin film structure at intermediate film thickness. We note that the slope across the edges between neighboring terraces appears highly exaggerated in the SFM height images (Fig. 5). This slope is determined by an interplay of the surface tension and the energetic penalty of creating a film with an unfavorable film thickness. While this penalty should decrease with in-

creasing dilution of the polymer, the surface tension should be only moderately affected, since this value is similar for the solvent and the polymer. The use of solvent in this way reduces the slope across the edges and stabilizes the nonfavorable microdomain structure $C_{\perp}$. In fact, the maximum slope amounts to only some 5° in the thinnest films between T0 and T1 and 3° between terrace T1 and T2. Over a lateral distance of a single cylinder diameter the film thickness varies therefore at most about 3 nm. Therefore, we may safely exclude the gradient in film thickness as an important driving force for the formation of upright cylinders.

A perforated lamella (PL) is found at high polymer concentrations and at a film thickness close to one or two layers of cylinders. The natural thickness of the PL phase seems to be somewhat larger than the one of the $C_{\parallel}$ phase, since it appears at the rim of holes at intermediate polymer concentrations. We emphasize that the perforated lamella is not a stable bulk structure of the SBS material, but is induced by the presence of the two boundary surfaces. Both the planar symmetry of the boundary surfaces and their preference to the majority (PB) phase lead to the stabilization of a ''nonbulk structure,'' also referred to as a ''surface reconstruction.''[24] Simulation results show that the surface field favors accumulation of PB at the homogeneous surfaces of the film, thereby depleting the center of the film of the majority phase.[50] As a consequence, the PS density increases in this portion of the film, leading to the formation of a continuous PS structure perforated by isolated PB channels. DDFT simulation results predict[49,50] that an even stronger surface field eventually should lead to the formation of a complete PS lamella in the center of the film. In our experiments, however, this effect was not observed. This is probably due to the fact that the experimentally accessible surface fields are limited in our system and cannot exceed the surface field of SBS without solvent. We find that for thicker films ($T2_h$) the PL phase appears only at the highest polymer concentrations Φ_p (see also Fig. 10). This resembles the DDFT simulation results of Horvat *et al.*[50] and can be interpreted in the following way. The solvent is expected to screen the interactions both between the two polymeric components and at the interfaces, higher polymer concentrations correspond to a stronger surface field. Therefore, the effective surface field acting on the topmost layer of the film is stronger in thinner films. This finding indicates that the two surface fields of both confining surfaces exhibit a characteristic decay length of the order of a microdomain spacing.[21] In thin enough films the effects of both surfaces can add and thereby stabilize the PL structure already at lower polymer concentrations.

We note that the PL phase was observed before in the bulk[66,67] as well as in thin films.[38] While in bulk the PL is considered to be metastable,[68] both our experiments and the DDFT simulations,[49,50] indicate that the existence of one or two planar interfaces preferentially attracting the majority phase stabilizes this structure.

At a film thickness below about one-fourth of the cylinder–cylinder distance, we observe in terrace T0 a grainy, disordered surface structure. Such a structure was also observed by Henkee *et al.*,[42] who reasoned that microphase separation is suppressed by the confinement. An alternative explanation is that terrace T0 consists of strongly adsorbed polymers, in which molecules are pinned to the substrate and their mobility is too low to rearrange during solvent vapor annealing.[69] The third possibility is the presence of a wetting layer or a half lamella as reported by Karim *et al.*,[20] which would imply that the SiO_x surface preferentially attracts PS. The existence of an absorbed layer or a wetting layer has implications regarding the surface field acting on the remaining copolymer film. Given the copolymer composition of $f_{PB}=0.74$, any adsorbed layer will exhibit preferential attraction to PB. Similarly a wetting layer will form such that PS is located close to the substrate exposing PB to the inside of the film. Such a layer would also exhibit preferential attraction to PB for the rest of the film. Since the free surface of the film preferentially attracts PB, corresponding to the lower surface energy of PB (see above), qualitatively symmetric boundary conditions are established. The excellent agreement between the experimental results and the DDFT simulations performed with symmetric boundary surfaces[49,50] corroborates this conclusion. However, the strength of the surface field cannot be expected to be equal at the free surface and at the film–substrate interface.

The DDFT simulations[49,50] predict a disordered phase for the thinnest films. For a strong preference of the minority block to the surfaces, a wetting layer is predicted. As chain adsorption onto the boundary surfaces is not captured by the simulations, a direct comparison between experiment and simulations seems questionable in this thickness regime. Also taking into account two dissimilar interfaces is probably essential to model such very thin films. For an in-depth discussion of the microdomain structure of the thinnest films, we refer to Refs. 50 and 70.

V. CONCLUSION

We have studied the phase behavior in thin films of a SBS block copolymers swollen in chloroform vapor. Both, the film thickness h_{wet} and the polymer volume fraction Φ_p were varied and a phase diagram of surface structures was established.

(1) The variation of Φ_p can be interpreted as a variation of the molecular interactions between the two polymer components and between the components and the boundary surfaces.
(2) The surface field causes cylinders to align parallel to the plane of the film, whenever the thickness fits an integer multiple of cylinder layers. At intermediate thickness the cylinders align perpendicular to the film plane. At higher polymer concentration, i.e., at stronger surface fields, a perforated lamella (PL) of PS forms. The surface field needed for PL formation increases with increasing film thickness. This corroborates simulation results that indicate a decay length of the surface field of about one microdomain spacing.[21,22,49,50]
(3) A wetting layer exists underneath all films, which either consists of pinned molecules or of a half lamella.

(4) The experimental results are in excellent agreement with computer simulations based on dynamic density functional theory.[49,50]

Both the experimental findings and the computer simulations indicate that the phase behavior of thin block copolymer films is governed by an interplay between surface fields and confinement effects. The preferential attraction of one of the two blocks to the surface (the surface field) can induce alignment as well as structural changes in the near-surface regions, socalled *surface reconstructions*. Confinement to a particular film thickness may imply compression/stretching of the respective structures, which involves additional entropic contributions to the free energy of the system. The interplay between both effects defines the stability range of the different surface structures.

ACKNOWLEDGMENTS

The authors acknowledge the help of M. Hund, discussions with A. Horvat, L. A. Tsarkova, A. V. Zvelindovsky, G. J. A. Sevink, and K. S. Lyakhova, the help of L. A. Tsarkova, A. Böker, S. Ludwigs, K. Schmidt, F. Schubert, and H. Zettl with the SAXS measurements, and financial support through the Deutsche Forschungsgemeinschaft (SFB 481). R.M. acknowledges support from the VolkswagenStiftung.

[1] P. Mansky, P. Chaikin, and E. L. Thomas, J. Mater. Sci. **30**, 1987 (1995).
[2] M. Park, C. Harrison, P. M. Chaikin, R. A. Register, and D. H. Adamson, Science **276**, 1401 (1997).
[3] K. W. Guarini, C. T. Black, Y. Zhang, H. Kim, E. M. Sikorski, and I. V. Babich, J. Vac. Sci. Technol. B **20**, 2788 (2002).
[4] C. T. Black, K. W. Guarini, K. R. Milkove, S. M. Baker, T. P. Russell, and M. T. Tuominen, Appl. Phys. Lett. **79**, 409 (2001).
[5] M. Park, P. M. Chaikin, R. A. Register, and D. H. Adamson, Appl. Phys. Lett. **79**, 257 (2001).
[6] J. Y. Cheng, C. A. Ross, V. Z. H. Chan, E. L. Thomas, R. G. H. Lammertink, and G. J. Vancso, Adv. Mater. (Weinheim, Ger.) **13**, 1174 (2001).
[7] T. Thurn-Albrecht, R. Steiner, J. DeRouchey, C. M. Stafford, E. Huang, M. Bal, M. Tuominen, C. J. Hawker, and T. P. Russell, Adv. Mater. (Weinheim, Ger.) **12**, 787 (2000).
[8] T. Thurn-Albrecht, J. Schotter, G. A. Kastle, N. Emley, T. Shibauchi, L. Krusin-Elbaum, K. Guarini, C. T. Black, M. T. Tuominen, and T. P. Russell, Science **290**, 2126 (2000).
[9] R. R. Li, P. D. Dapkus, M. E. Thompson, W. G. Jeong, C. Harrison, P. M. Chaikin, R. A. Register, and D. H. Adamson, Appl. Phys. Lett. **76**, 1689 (2000).
[10] F. S. Bates and G. H. Fredrickson, Phys. Today **52**, 32 (1999).
[11] F. S. Bates and G. H. Fredrickson, Annu. Rev. Phys. Chem. **41**, 525 (1990).
[12] J. W. Hamley, *The Physics of Block Copolymers* (Oxford University Press, Oxford, 1998).
[13] T. Hashimoto, H. Tanaka, and H. Hasegawa, Macromolecules **23**, 4378 (1990).
[14] U. Jeong, H.-C. Kim, R. L. Rodriguez, I. Y. Tsai, C. M. Stafford, J. K. Kim, C. J. Hawker, and T. P. Russell, Adv. Mater. (Weinheim, Ger.) **14**, 274 (2002).
[15] T. L. Morkved, M. Lu, A. M. Urbas, E. E. Ehrichs, H. M. Jaeger, P. Mansky, and T. P. Russell, Science **273**, 931 (1996).
[16] R. A. Segalman, H. Yokoyama, and E. J. Kramer, Adv. Mater. (Weinheim, Ger.) **13**, 1152 (2001).
[17] J. Heier, J. Genzer, E. J. Kramer, F. S. Bates, S. Walheim, and G. Krausch, J. Chem. Phys. **111**, 11101 (1999).
[18] G. H. Fredrickson, Macromolecules **20**, 2535 (1987).
[19] H. Yokoyama, T. E. Mates, and E. J. Kramer, Macromolecules **33**, 1888 (2000).
[20] A. Karim, N. Singh, M. Sikka, F. S. Bates, W. D. Dozier, and G. P. Felcher, J. Chem. Phys. **100**, 1620 (1993).
[21] H. P. Huinink, J. C. M. Brokken-Zijp, M. A. van Dijk, and G. J. A. Sevink, J. Chem. Phys. **112**, 2452 (2000).
[22] H. P. Huinink, M. A. van Dijk, J. C. M. Brokken-Zijp, and G. J. A. Sevink, Macromolecules **34**, 5325 (2001).
[23] M. S. Turner, M. Rubinstein, and C. M. Marques, Macromolecules **27**, 4986 (1994).
[24] N. Rehse, A. Knoll, M. Konrad, R. Magerle, and G. Krausch, Phys. Rev. Lett. **87**, 035505 (2001).
[25] N. Rehse, A. Knoll, R. Magerle, and G. Krausch, Macromolecules **36**, 3261 (2003).
[26] G. Coulon, T. P. Russell, V. R. Deline, and P. F. Green, Macromolecules **22**, 2581 (1989).
[27] M. A. van Dijk and R. van den Berg, Macromolecules **28**, 6773 (1995).
[28] P. Lambooy, T. P. Russell, G. J. Kellogg, A. M. Mayers, P. D. Gallagher, and S. K. Satija, Phys. Rev. Lett. **72**, 2899 (1994).
[29] D. G. Walton, G. J. Kellogg, A. M. Mayes, P. Lambooy, and T. P. Russell, Macromolecules **27**, 6225 (1994).
[30] G. J. Kellogg, D. G. Walton, A. M. Mayes, P. Lambooy, T. P. Russell, P. D. Gallagher, and S. K. Satija, Phys. Rev. Lett. **76**, 2503 (1996).
[31] M. J. Fasolka, P. Banerjee, A. M. Mayes, G. Pickett, and A. C. Balazs, Macromolecules **33**, 5702 (2000).
[32] M. J. Fasolka and A. M. Mayes, Ann. Rev. Mater. Res. **31**, 323 (2001).
[33] S. N. Magonov, J. Cleveland, V. Elings, D. Denley, and M.-H. Whangbo, Surf. Sci. **389**, 201 (1997).
[34] G. Kim and M. Libera, Macromolecules **31**, 2670 (1998).
[35] G. Kim and M. Libera, Macromolecules **31**, 2569 (1998).
[36] H.-C. Kim and T. P. Russell, J. Polym. Sci., Part B: Polym. Phys. **39**, 663 (2001).
[37] Z. Lin, D. H. Kim, X. Wu, L. Boosahda, D. Stone, L. LaRose, and T. P. Russell, Adv. Mater. (Weinheim, Ger.) **14**, 1373 (2002).
[38] L. H. Radzilowski, B. L. Carvalho, and E. L. Thomas, J. Polym. Sci., Part B: Polym. Phys. **34**, 3081 (1996).
[39] M. Konrad, A. Knoll, G. Krausch, and R. Magerle, Macromolecules **33**, 5518 (2000).
[40] C. Harrison, M. Park, P. M. Chaikin, R. A. Register, D. H. Adamson, and N. Yao, Macromolecules **31**, 2185 (1998).
[41] Q. Zhang, O. K. C. Tsui, B. Du, F. Zhang, T. Tang, and T. He, Macromolecules **33**, 9561 (2000).
[42] C. S. Henkee, E. L. Thomas, and L. J. Fetters, J. Mater. Sci. **23**, 1685 (1988).
[43] G. J. A. Sevink, J. G. E. M. Fraaije, and H. P. Huinink, Macromolecules **35**, 1848 (2002).
[44] G. G. Pereira, Phys. Rev. E **63**, 061809 (2001).
[45] Q. Wang, P. F. Nealey, and J. J. de Pablo, Macromolecules **34**, 3458 (2001).
[46] G. Szamel and M. Müller, J. Chem. Phys. **118**, 905 (2003).
[47] J. Feng and E. Ruckenstein, Macromol. Theory Simul. **11**, 630 (2002).
[48] J. Feng, H. Liu, and Y. Hu, Macromol. Theory Simul. **11**, 556 (2002).
[49] A. Knoll, A. Horvat, K. S. Lyakhova, G. Krausch, G. J. A. Sevink, A. V. Zvelindovsky, and R. Magerle, Phys. Rev. Lett. **89**, 035501 (2002).
[50] A. Horvat, K. S. Lyakhova, G. J. A. Sevink, A. V. Zvelindovsky, and R. Magerle, J. Chem. Phys. **120**, 1117 (2004), following paper.
[51] J. Brandrup and E. H. Immergut, *Polymer Handbook* (Wiley, New York, 1989).
[52] H. Elbs, thesis, University of Bayreuth, 2001.
[53] Note that in Ref. 49 the vapor pressure was estimated by the ratio of saturated to pure gas flow as determined by the flow meters used. These estimated values deviate up to 20% at high Φ_p from the vapor pressure p given in Fig. 3 of the present work, where p was controlled more accurately via the temperature of the solvent bath.
[54] G. H. Fredrickson and L. Leibler, Macromolecules **22**, 1238 (1989).
[55] P. J. Flory, *Principles of Polymer Chemistry*, 3rd ed. (Cornell University Press, Ithaca, 1989).
[56] A. Knoll, A. Horvat, K. S. Lyakhova, G. Krausch, G. J. A. Sevink, A. V. Zvelindovsky, and R. Magerle (unpublished).
[57] POV-Team (1991–2002).
[58] R. Magerle, Phys. Rev. Lett. **85**, 2749 (2000).
[59] A. Knoll, R. Magerle, and G. Krausch, Macromolecules **34**, 4159 (2001).
[60] M. W. Matsen and F. S. Bates, J. Chem. Phys. **106**, 2436 (1997).
[61] S. Wu, J. Phys. Chem. **74**, 632 (1970).
[62] B. B. Sauer and N. V. Dipaolo, J. Colloid Interface Sci. **144**, 527 (1991).

[63] K. J. Hanley and T. P. Lodge, J. Polym. Sci., Part B: Polym. Phys. **36**, 3101 (1998).
[64] T. Hashimoto, M. Shibayama, and H. Kawai, Macromolecules **16**, 1093 (1983).
[65] T. P. Lodge, C. Pan, X. Jin, Z. Liu, J. Zhao, W. W. Maurer, and F. S. Bates, J. Polym. Sci., Part B: Polym. Phys. **33**, 2289 (1995).
[66] A. K. Khandpur, S. Foerster, F. S. Bates, I. W. Hamley, A. J. Ryan, W. Bras, K. Almdal, and K. Mortensen, Macromolecules **28**, 8796 (1995).
[67] S. Foerster, A. K. Khandpur, J. Zhao, F. S. Bates, I. W. Hamley, A. J. Ryan, and W. Bras, Macromolecules **27**, 6922 (1994).
[68] D. A. Hajduk, H. Takenouchi, M. A. Hillmyer, and F. S. Bates, Macromolecules **30**, 3788 (1997).
[69] C. Harrison, P. M. Chaikin, D. A. Huse *et al.*, Macromolecules **33**, 857 (2000).
[70] K. S. Lyakhova, A. Horvat, R. Magerle, G. J. A. Sevink, and A. V. Zvelindovsky, J. Chem. Phys. (to be published).